Accepted Manuscript

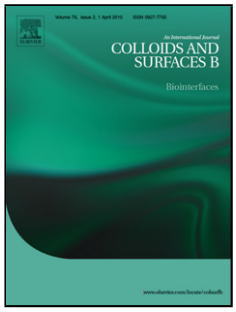

Title: Bacterial Cellulose Hydrogel Loaded with Lipid Nanoparticles for Localized Cancer Treatment

Authors: M.L. Cacicedo, G.A. Islan, I.E. León, V.A. Álvarez, I. Chourpa, E. Allard-Vannier, N. García-Aranda, Z.V. Díaz-Riascos, Y. Fernández, S. Schwartz Jr, I. Abasolo, G.R. Castro

PII: S0927-7765(18)30427-2
DOI: https://doi.org/10.1016/j.colsurfb.2018.06.056
Reference: COLSUB 9446

To appear in: *Colloids and Surfaces B: Biointerfaces*

Received date: 26-3-2018
Revised date: 14-6-2018
Accepted date: 25-6-2018

Please cite this article as: Cacicedo ML, Islan GA, León IE, Álvarez VA, Chourpa I, Allard-Vannier E, García-Aranda N, Díaz-Riascos ZV, Fernández Y, Schwartz S, Abasolo I, Castro GR, Bacterial Cellulose Hydrogel Loaded with Lipid Nanoparticles for Localized Cancer Treatment, *Colloids and Surfaces B: Biointerfaces* (2018), https://doi.org/10.1016/j.colsurfb.2018.06.056

Bacterial Cellulose Hydrogel Loaded with Lipid Nanoparticles for Localized Cancer Treatment

M. L. Cacicedo[a], G. A. Islan[a], I. E. León[b], V. A. Álvarez[c], I. Chourpa[d], E. Allard-Vannier[d], N. García-Aranda[e f g], Z. V. Díaz-Riascos[e g], Y. Fernández[e f g], S. Schwartz Jr. [f g *], I. Abasolo[e f g *], G. R. Castro[a *]

a. Nanobiomaterials Lab, CINDEFI, School of Sciences, National University of La Plata-CONICET (CCT La Plata), 50 & 115 street. CP 1900 AJL City of La Plata, Buenos Aires, Argentina. *Email: grcastro@gmail.com

b. Chemical Inorganic Center (CEQUINOR, UNLP, CONICET), School of Sciences, National University of La Plata-CONICET (CCT La Plata). CP 1900 AJL City of La Plata, Buenos Aires, Argentina.

c. CoMP (Composite Materials Group), Research Institute of Material Science and Technology (INTEMA), Engineering School, National University of Mar del Plata, Av. Colón 10890, (B7608FDQ) Mar del Plata, Argentina

d. Université Francois-Rabelais de Tours, EA6295 "Nanomedicaments et Nanosondes", 31 Avenue Monge, 37200, Tours, France

e. Functional Validation & Preclinical Research (FVPR), CIBBIM-Nanomedicine, Vall d'Hebron Institut de Recerca (VHIR), Universitat Autònoma de Barcelona (UAB), 08035 Barcelona, Spain. *Email: ibane.abasolo@vhir.org

f. Drug Delivery & Targeting Group, CIBBIM-Nanomedicine, Vall d'Hebron Institut de Recerca (VHIR), Universitat Autònoma de Barcelona (UAB), 08035 Barcelona, Spain. *Email: simo.schwartz@vhir.org

g. Networking Research Center on Bioengineering, Biomaterials and Nanomedicine (CIBER-BBN), Barcelona, Spain

Graphical abstract

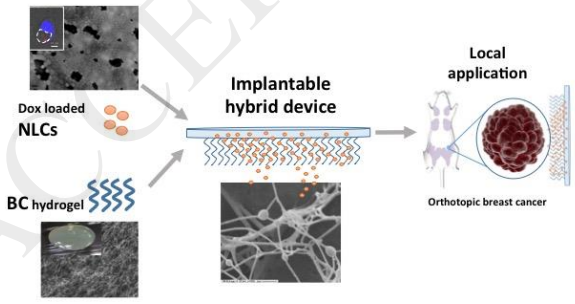

HIGHLIGHTS

- Cationic state of the Dox in NLCs determined drug release and in vitro efficacy
- NLCs with cationic and neutral Dox were loaded into bacterial cellulose (BC)
- The hybrid BC-NCL-NH system was efficacious inhibiting tumor growth and metastasis
- BC-NLCs-NH eradicated the side effects of intratumorally administered Dox

Abstract

The use of hybrid materials, where a matrix sustains nanoparticles controlling the release of the chemotherapeutic drug, could be beneficial for the treatment of primary tumors prior or after surgery. This localized chemotherapy would guarantee high drug concentrations at the tumor site while precluding systemic drug exposure minimizing undesirable side effects.

We combined bacterial cellulose hydrogel (BC) and nanostructured lipid carriers (NLCs) including doxorubicin (Dox) as a drug model. NLCs loaded with cationic Dox (NLCs-H) or neutral Dox (NLCs-N) were fully characterized and their cell internalization and cytotoxic efficacy were evaluated *in vitro* against MDA-MB-231 cells. Thereafter, a fixed combination of NLCs-H and NLCs-N loaded into BC (BC-NLCs-NH) was assayed *in vivo* into an orthotopic breast cancer mouse model.

NLCs-H showed low encapsulation efficiency (48%) and fast release of the drug while NLCs-N showed higher encapsulation (97%) and sustained drug release. Both NLCs internalized via endocytic pathway, while allowing a sustained release of the Dox, which in turn rendered IC50 values below of those of free Dox. Taking advantage of the differential drug release, a mixture of NLCs-N and NLCs-H was encapsulated into BC matrix (BC-NLCs-NH) and assayed in vivo, showing a significant reduction of tumor growth, metastasis incidence and local drug toxicities.

Keywords: Drug delivery, bacterial cellulose, nanostructured lipid carriers, doxorubicin, breast cancer, localized chemotherapy, nanocomposite, neo-adjuvant therapy, hydrogel, controlled release.

1. INTRODUCTION

Cancer is the second worldwide cause of mortality accounting for 8.2 million deaths in 2012 [1]. Even though surgical tumor resection is the preferred treatment for solid localized tumors at early or intermediate stage, radiation and/or chemotherapy therapies are often employed to prevent recurrent tumor grow [2]. However, tumor location, size and stage may preclude this surgical approach in many patients dramatically reducing their survival [3]. Additionally, diffusion and efficacy of therapeutic drugs are far from optimal. Drug molecules injected systemically must travel longer distances from blood vessels to reach tumor cells (≥ 100 μm) compared with normal

tissues, and consequently, there is insufficient drug concentration and penetration at the tumor site [4]. Moreover, only about 10% to 15% of tumor cells population are expected to be within the mitotic phase of cell division when the drug reaches the tumor and therefore, its antitumor effect is often limited by the short circulation half-life of chemotherapeutic drugs [2,5,6]. In addition, surpassing multidrug resistance (MDR) is also a big challenge in chemotherapeutic treatments. MDR can be acquired during treatment due to an adaptive response of cancer cells to cytotoxic drugs, leading to treatment failure [7,8]. Therefore, high doses of chemotherapeutic agents are required, which further turns into drug-related toxicity [9]. In this sense, localized sustained release of chemotherapeutics could improve the treatments by ensuring an extended local exposure of tumor cells to drugs, while lowering systemic drug levels [10].

Biomaterials have been thoroughly investigated as platforms for efficient drug encapsulation and sustained release at the implantation site of localized chemotherapy [11]. Localized chemotherapy allows high drug concentrations at the tumor site for extended periods of time while keeping low systemic drug exposure. The potential advantages of local therapy are the reduction of undesirable side effects in the patients and lowering the chance of acquiring drug resistance in the long term [3]. Additionally, this treatment schemes reduce the need for repeated drug administrations. The implantation of this devise works as an adjuvant therapy, being possible to combine it with low-doses systemic administration of common chemotherapeutics [11]. Particularly, hydrogels are hydrophilic polymeric networks with tissue-like properties and applications on tissue engineering and drug delivery [12,13]. Among biopolymers, bacterial cellulose (BC) has been extensively studied [14]. BC is an extra-cellular polysaccharide synthesized in Gram-negative bacteria, like *Komagataeibacter hansenii*, and located at the interface of air/liquid culture. This cellulose is synthesized in nanofibrils composed of β-1→4 glucose units stabilized by inter- and intra-chain hydrogen bonds. BC hydrogels with nanofibrillar structure are composed of pure cellulose network containing more than 90% water, possess high mechanical strength and thermostability, and well-defined biocompatibility [15],[16]. Further, high flexibility and porosity (*i.e*. similar to collagen) makes BC an excellent biomaterial that could be used as matrix for localized drug delivery [14]. Moreover, BC can be purified reaching endotoxin values lower than 20 endotoxin units/device and is already approved by the FDA for implants [17]. Nevertheless, low molecular weight molecules can diffuse freely in and out of the BC membranes which results in undesirable burst release of most drugs [15].

On the other hand, drug delivery nanosystems have been widely developed in the last years aiming the improvement of the therapeutic index of marketed drugs by means of modifying their pharmacokinetics and biodistribution [18],[19]. Additionally, nanoparticle-based drug delivery systems could overcome drug resistance using a Trojan horse-like approach [7] to bypass the effect of the MDR machinery such as efflux pumps [20,21]. Among lipid nanosystems, nanostructured lipid carriers (NLCs) are a second generation of solid lipid nanoparticles evolved to improve some drawbacks such as close-fitting packaging among lipid molecules. This decreases the encapsulation efficiency (EE) of cargo molecules which are often extruded from the high crystalline structure of the nanoparticle. NLCs are composed by a mixture of solid and liquid lipids which generate imperfections within the matrix, decreasing its crystallinity and facilitating the accommodation of drug molecules. In this sense, improved drug encapsulation,

minimized drug leakage during storage and controlled drug release kinetics are expected [22,23]. Additional advantages of NCL include high biocompatibility and simple production at large scale [24]. NLCs have been gaining attention for delivery of commonly used chemotherapeutics such as doxorubicin (Dox) and cisplatin [25–27]. Moreover, lipid based nanocarriers have been described as valuable devices for drug delivery systems to overcome MDR in cancer cells [28–31].

The integration of both structures, BC and NLC, might help to develop hierarchical implantable matrices taking advantage of the positive role of each system. Once nanoparticles are embedded into a hydrogel a unique hybrid biomaterial is synthesized that could show extended drug release. Also, BC-NLC hybrid hydrogels can combine the properties of fast release of the free drug dispersed into polymeric network and long-term molecular release from the drug-loaded nanoparticles [12]. The relevance of using combinations of BC and nanoparticle has been recently highlighted in the work of Chu et al. where bacterial cellulose was used as a depot for C60 nanoparticles, an effective photosensitizer for photodynamic therapy in skin cancer [32].

In the present work, a novel hybrid biomaterial combining bacterial cellulose hydrogel and lipid nanoparticles was developed for its application as local drug delivery implant for cancer therapy using Dox. NLCs loaded with two forms of Dox were analyzed *in vitro* and *in vivo* using MDA-MB-231 breast cancer cell line and an orthotopic mouse model. In our hands, BC-NLCs-NH showed low levels of local and systemic toxicity as well as strong efficacy in tumor reduction and metastatic incidence. These results clearly reinforce the potential use of BC-NLCs-NH as local drug delivery system.

2. EXPERIMENTAL SECTION

2.1. Materials

The lipid myristyl myristate (Crodamol™ MM) and the oil (Crodamol™ GTCC-LQ) were kindly donated by Croda (Argentina). Doxorubicin hydrocloride (Dox, MW 579.98) was kindly supplied by LKM pharmaceuticals (Argentina). 3-(4,5-dimethylthiazol-2-yl)-2,5-diphenyltetrazolium bromide (MTT) and Pluronic®F68 were provided by Sigma-Aldrich (St. Louis, Mo, USA). All other reagents used were of analytical or microbiological grade purchased from Sigma-Aldrich or Merck (Darmstadt, Germany).

2.2. Nanostructured lipid carrier (NLC) preparation

NLCs containing Dox were prepared by sonication method [33]. Briefly, 400 mg of solid lipid (2.0%, w/v) were melted under water bath at 60°C and mixed with 10 mg of Dox (dissolved in 100 µL of DMSO). Liquid lipid (oil) (0.06%, v/v) was incorporated. After 10 min, a hot aqueous solution (20 mL) containing 3% (w/v) of Pluronic®F68 was added to the lipid phase. Immediately, the mixture was sonicated for 50 min (40% amplitude) using an ultrasonic processor (130 Watts, Cole-Parmer, USA) equipped with 3 mm titanium tip. Then, the dispersion was cooled at room temperature and stored at 5°C.

Two forms of Dox were used to prepare the NLCs. First, 10 mg/mL Dox hydrochloride was solubilized in 1.0 mM HCl solution (pH= 3.0, favoring dominance of the cationic drug, hereafter called Dox-H) and incorporated to NLCs (NLCs-H). Alternatively, the pH of a Dox solution was adjusted to 8.5 (hereafter called Dox-N). The ionic equilibrium of Dox is dynamic under the experimental conditions because is involved in several types of molecular interactions such as Π-Π stacking of the aromatic rings at high concentrations. Dox dimerization constant (Kd) depends directly on total drug concentration [34]. Moreover, after increasing the pH at 8.5, drug solubility decrease is considerable (from 20 mg/ml to 0,3 mg/ml) [35]. Consequently, equilibrium is displaced to the predominant form of neutral Dox in solution. Then, the solution was frozen at -80ºC and lyophilized. The Dox-N was used to prepare the NLC formulation (NLCs-N) using the same lipid composition as NLCs-H.

2.3. Measurement of free Dox and Dox loading efficiency in NLCs

After NLCs synthesis, the final reaction volume was measured (evaporation occurred during sonication procedure). Samples of 500 µL were then transferred to ultrafiltration centrifugal device (MWCO 10,000, Microcon, Millipore, MA, USA) and centrifuged at 5,000 ×g for 10 min to retain the NLCs. The filtrate was 10-times diluted in 10 mM phosphate buffer to measure the non-encapsulated Dox by fluorimetry (PerkinElmer LS 50B, Japan). The encapsulation efficiency (EE) was calculated as follows:

$$EE\ (\%)\ = \frac{(Qo\ -\ (Cr\ x\ V))\ X\ 100}{Qo}$$

Where, *Qo* is initial amount of Dox, *Cr* is concentration of Dox in the filtered solution, and *V* is the final volume after finishing the preparation.

Additionally, the total amount of Dox in each formulation was analyzed. First, 450 µL of methanol was added to 100 µL of NLCs. Then, 450 µL of chloroform was incorporated and centrifuged at 10,000 ×g for 10 min. The supernatant was diluted 10-times with a methanol/chloroform mixture (50:50) and the total Dox was measured.

Dox was quantified by fluorimetry using λ_{ex}= 476 nm and λ_{em}= 588 nm, according the appropriate calibration curve in the range of 2.5 to 12.5 µM.

2.4. Particle size, zeta potential and poly-dispersity index (PDI)

The average diameter and size distribution of lipid nanoparticles were measured by photon correlation spectroscopy (PCS) (Nano ZS Zetasizer, Malvern Instruments Corp, UK) at 25ºC in polystyrene cuvettes with a thickness of 10 mm. The zeta potential was determined by laser Doppler anemometry also using the Nano ZS Zetasizer. The zeta potential measurements were performed in capillary cells, for the NPs dispersed in deionized water obtained from Milli-Q system (Millipore, MA, USA). Also, the PDI value was determined. All the measurements were carried out in triplicate.

2.5. Drug release assays

Experiments were performed using dialysis membranes (MWCO 10 kDa.). The membranes were soaked with distilled water for 12 h and filled with 5.0 mL of each formulation of NLCs, followed by immersion in 30 mL of 10 mM acetate buffer (pH= 5.0) or 10 mM phosphate buffer (pH= 7.4) at 37°C, with continuous shaking at 200 rpm. At different times, samples of 10 mL were withdrawn and Dox concentration was measured in a fluorimeter, as explained above.

2.6. Physicochemical characterizations

2.6.1. Thermogravimetric analysis (TGA)

Dynamic thermogravimetric measurements of the nanoparticles were performed by using a Shimadzu TGA-50 instrument (Tokyo, Japan). Tests were run in the range of 0ºC to 600ºC at a heating rate of 10ºC/min under N_2 atmosphere.

2.6.2. Differential scanning calorimetry (DSC)

Thermal properties of NLCs particles were determined by differential scanning calorimetry (DSC, PerkinElmer Inc., Model Pyris 1, Waltham, MA, USA) under nitrogen atmosphere. Scans were carried out at a heating rate of 10ºC min^{-1} in the 20ºC - 240ºC temperature range.

2.6.3. X-ray Diffraction analysis (XRD)

XRD patterns were collected in reflection mode on a glass substrate, and analyzed by Origin and Sigma Plot software. The measurement was performed with an Analytical Expert instrument using Cu-K_α radiation (λ= 1.54 Å) from 2θ= 10º to 60º in continuous mode with 0.07º step size. Scattering angles were transformed into short spacing using Bragg's equation: $2d (\sin \Theta) = n \lambda$.

2.7. Microscopic studies

2.7.1. Scanning electron microscopy (SEM)

Samples were placed in glass slides and dried by the critic point technique. After that, the surface was sputtered with gold using a metalizer (BalzersSCD 030), obtaining a layer thickness in the range of 15 to 20 nm. Film surfaces and morphologies were observed by SEM (Philips SEM 505 model, Rochester, NY, USA). The images were processed by an image digitizer program (Soft Imaging System ADDA II).

2.7.2. Transmission electron microscopy (TEM)

The nanoparticle dispersion was 10-times diluted with ultrapure water and a drop of the dispersion was spread onto a collodion-coated Cu grid (400-mesh). Liquid excess was drained with paper filter (Whatman #1) and for contrast enhancement a drop of phosphotungstic acid as added to the NLCs dispersion. Finally, TEM analysis was performed using Jeol-1200 EX II-TEM microscope (Jeol, MA, USA).

2.8. *In vitro* assays

2.8.1. Cell culture

Breast cancer cell line MDA-MB-231 was obtained from the American Type Culture Collection (ATCC® HTB-26™, LGC Standards, Barcelona, Spain), and cultured in Dulbecco's modified Eagle's medium (DMEM/F12; Invitrogen, Paisley, UK) supplemented with 10% fetal bovine serum (FBS; Lonza, Barcelona, Spain), 1% penicillin-streptomycin, 1% L-Glutamine, 1% non-essential amino acids and 1% sodium pyruvate (Life Technologies, Madrid, Spain). Cells were maintained in an atmosphere with 5% CO_2 and 95% humidified atmosphere air at 37°C.

2.8.2. Internalization assay

Cells were seed for 24 h in standard 24-well plates at 8×10^4 cells *per* well to test the free Dox internalization kinetic, NLCs-N and NLCs-H. It was used an equivalent Dox concentration of 0.625 μM. After drug exposition for 0.5, 1, 2, 3 and 6 h cells were washed twice with PBS. Then, were treated with trypsin and 1.0 mL of medium was added to each well. After that, samples were collected in cytometry tubes and centrifuged at 2500 xg for 5 min. Supernatant was discarded and cells were re-suspended in 350 μL of PBS. Fluorescence intensity was monitored using a FACSCalibur (Becton–Dickinson, Franklin Lakes, NJ, USA) and analyzed using FCS Express 3.0 software (De Novo Software, Los Angeles, CA, USA).

2.8.3. Cytotoxicity tests

Cytotoxicity of NLC samples were performed in MDA-MB-231 cells seeded for 24 h in standard 96-well plates at 6×10^3 cells *per* well. Cells were treated for 72 h with medium containing different Dox equivalent concentrations (0.0061–100 μM) of the following compounds: free Dox, NLCs-N and NLCs-H. After the incubation, cells were washed with PBS and fresh medium added. Cell viability was determined using a tetrazolium dye (MTT) assay as previously described [36]. Briefly, cells were incubated for 4 h containing 0.5 g L^{-1} of MTT, and the medium replaced with DMSO to dissolve the formazan crystals formed by viable cells. Absorbance was measured at 540 nm using a multi-well plate reader (ELX800, Biotek, France). The inhibitory concentration (IC_{50}) was determined as the drug concentration that resulted in a 50% reduction in cell viability after fitting a dose response curve (GraphPad Prism 6 software, San Diego, CA, USA). Results were expressed as a mean of three independent experiments.

2.8.4. Confocal microscopy

MDA-MB-231 cells were plated in collagen-coated cover glasses on 24 well-plates at density of 100,000 cells mL^{-1} of DMEM/F12 with 10% FBS and incubated at 37ºC for 24 h. Thereafter, cells were exposed to free Dox and NLCs-N at a concentration of 10 μM. After 2 h incubation, medium was discharged and cells were washed with PBS. Next, Lysotracker Green (20 μM, Invitrogen, MA, USA) was added to each well and incubated at 37ºC for 30 min. Cells were washed and counterstained with Hoechst 33342 (Sigma-Aldrich, MO, USA) prior to their visualization by confocal laser scanning microscope (Olympus FV1000 Confocal and Spectral Microscope, Japan).

2.8.5. Fluorescence confocal spectral imaging (FCSI)

MDA-MB-231 cells adherent to poly-D-lysine coated cover glasses were grown in 24-well plates and incubated with NLCs-N at 1.0 μM Dox for 1 h or 22 h. After washing them three times with fresh PBS, the cover glasses were placed between a microscope slide and a cover slip to be scanned for FCSI using a LabRAM laser scanning confocal microspectrometer (Horiba, Villeneuve d'Ascq, France), equipped with a 300 '/mm diffraction grating and a CCD detector air-cooled by Peltier effect. The Dox fluorescence was excited using 491 nm line of a solid laser (Cobolt, model Calypso 75), under a long focal microscope objective 50×. The equatorial optical section of each selected cell was scanned with a step of 0.8 μm and the full fluorescence spectrum has been recorded for each scanned point (typically 30×30 = 900 spectra per cell optical section). The laser light power at the sample was ca. 0.2 mW and the acquisition time was 0.05 sec per spectrum. Both acquisition and treatment of spectral maps were performed using LabSpec software. The spectral maps were generated as described elsewhere [37]. Briefly, each fluorescence spectrum has been fitted with a proportional sum of model spectra characteristic of subcellular locations and/or interactions. The fitting coefficients were used to generate the corresponding spectral maps shown with pseudo colors.

2.9. Preparation of the biopolymeric matrix: NLCs loading and release

The synthesis of bacterial cellulose (BC) by *K. hansenii* (ATCC 23769) was performed in a medium containing (g L^{-1}): 25.0 mannitol, 5.0 yeast extract, 3.0 peptone, and adjusted to pH 6.5 with 100 mM NaOH solution before sterilization. The culture was maintained statically in 48-well plates at 30ºC for 10 days. The BC films were collected from the plates and washed with distilled water. BC purification was performed incubating the membranes in 100 mM NaOH at 50ºC for 24 h followed by successive washes with distilled water, thereafter the pH was adjusted to 7.0. Later, the BC films were sterilized by autoclaving (121ºC for 20 min). Next, BC films were loaded with free Dox (BC-Dox), NLCs-N (BC-NLCs-N) and a mix of NLCs-N and NLCs-H in a 20:80 ratio (BC-NLCs-NH), respectively.

Loading assays of BC films were performed by immersion in the corresponding 1.0 mM Dox solutions. After 24 h incubation, the films were washed with physiologic solution followed by Dox extraction using organic solvents. First, BC films were immersed in methanol for 2 h followed by an immersion in methanol/chloroform (50:50) for another 2 h. Finally, one more methanol immersion was performed for 2 h. Total Dox was quantified by fluorimetry.

Dox kinetic release from BC loaded films was analyzed by soaking the films into 2 mL-tubes containing 1.5 mL of physiologic solution at 37ºC. Samples of 200 μL were taken out from the tubes at different times and Dox was quantified by fluorescence. The assays were performed by quadruplicate for 35 days and results expressed as a mean of two independent experiments.

2.10. *In vivo* tumorigenic assays

Female athymic nude mice (Envigo Crs. S.A., Barcelona, Spain) were kept in pathogen-free conditions and used at 7 weeks of age. Animal care was handled in accordance with the Guide for the Care and Use of Laboratory Animals of the Vall d´Hebron University Hospital Animal Facility, and the experimental procedures were approved by the Animal Experimentation Ethical

Committee at the institution. *In vivo* studies were performed by the ICTS "NANBIOSIS", at the CIBER-BBN's *in vivo* Experimental Platform of the Functional Validation & Preclinical Research (FVPR) area (http://www.nanbiosis.es/portfolio/u20-in-vivo-experimental-platform/) (Barcelona, Spain).

MDA-MB-231.Fluc cells (2×10^6) suspended in 200 µL of PBS with Matrigel (1:1) (BD Bioscience, Bedford, MA, USA) were implanted into the right abdominal mammary fat pad (i.m.f.p.). Tumor growth was monitored twice a week by conventional caliper measurements ($D \times d^2/2$, where D is the major diameter and d the minor diameter). After sixteen days post-tumor inoculation, a circular BC film (∅= 12 mm) loaded with a mix of NLCs-N and NLCs-H in a 20:80 ratio (BC-NLCs-NH), respectively, and containing a Dox loading of 0.14 mg was placed at the primary tumor site during a second surgery that placed the film between the tumor-bearing mammary fat pad and the abdominal wall. The control groups consisted of a free Dox intratumorally injected group (0.14 mg in 25 µL as a unique dose) and a non-treated one (n= 9/group). During treatment, supervision of the animals and body weight measurement were performed twice a week. Clinical observations included changes in skin, eyes, mucous membranes, alterations in respiratory pattern, behavior, posture, response to handling and the presence of abnormal movements. At the end of experiment, primary tumors, lungs and heart were excised and weighted. Tissues were cleaned with PBS, fixed in 4% formaldehyde solution and embedded in paraffin.

2.11. Statistical analysis

Statistical analyses and graphs were performed using GraphPad Prism 6 software. If not said otherwise, all error bars in figures correspond to standard deviation (SD) The significance threshold was established at $p<0.05$, and significance levels were schematically assigned *($0.01 \leq p < 0.05$), **($0.001 \leq p < 0.01$) or ***($0.0001 \leq p < 0.001$).

3. RESULTS AND DISCUSSION

3.1. NLCs synthesis and characterization

Colloidal drug delivery system based on NLC was selected as a suitable Dox carrier. Encapsulation was performed considering the different ionic states of the anthracycline in equilibrium and the predominance of each form depending on the surrounding pH (**Scheme 1**) [38]. Once Dox hydrochloride was solubilized, the molecule exists as a monocation (Dox-H). The specific pKa for Dox primary amine deprotonation is 8.46 [38,39]. During encapsulation experiments, the residual charge of Dox could determine the interaction within the matrix components and probably determine the drug release kinetic. In this sense, there were obtained two forms of the drug: the monocation (Dox-H) and a predominance of neutral Dox species (Dox-N) by adjusting the pH solution (**Scheme 1**). Later, both forms of Dox were incorporated in the lipid phase and by ultra-sonication method two NLCs formulations with different characteristics

were observed, named NCL-H or NCL-N depending on their cargo, Dox-H or Dox-N, respectively.

Dox EE showed significant differences between the NLC-H and NLC-N formulations **(Table 1)**. NLCs synthesis containing Dox-N exhibited a high EE (96.6%), due to the more hydrophobic character of both matrix and drug. On the other hand, NLCs-H synthesis produced a two times decrease on EE (value of 48.0%) which points out that 52% of Dox-H was not encapsulated and remains free in the formulation.

Analysis of both types of NLC by DLS and zeta potential confirmed similar values of around 150 nm for hydrodynamic diameter and +2.5 mV for the surface charge (**Table 1**). The size and the slightly positive charge of the nanoparticles suggested good properties for cell internalization [40]. Further, polydispersity (PDI) values indicate a nearly mono-dispersed nanoparticles suspension for both systems with a very uniform size distribution (**Table 1** and **Figure S1**). These results suggest that the difference on Dox charge (Dox-H or Dox-N) does not interfere with NLCs size and morphology.

Morphology and size distribution of NLCs were also studied by TEM microscopy (**Figures 1A & 1B**). Images showed a pretty narrow size-distribution of nanoparticles with spherical shape and mean diameters below 150 nm, either for NLCs-N and NLCs-H in agreement with DLS experiments (**Table 1**). TGA analysis of NLCs has been depicted showing the TGA derivative (DTGA) curves (**Figure 1C**) or the original TGA curves (**Figure S2B**). DTGA gave specific information about the inflexions found in decomposition thermograms **(Figure 1C)**. In this sense, a strong inflexion at 187ºC was noticed. This temperature value corresponded to Dox melting temperature, also confirmed by DSC analysis (**Figure S2A**). The thermograms (DTGA) showed shifts on two peaks, especially one in the range 200ºC - 300ºC which could be attributed to myristyl myristate decomposition [41], suggesting that the second step at 398.7ºC observed on TGA curves correspond to oil decomposition temperature (**Figure S2B**). These results confirm the presence of two components, lipid and oil, in the nanoparticles. Both NLCs-N and NLCs-H exhibited a shift from 398.7ºC to 385.0ºC in comparison with empty NLCs. No peak corresponding to Dox melting was observed neither for NLCs-N nor NLCs-H. Moreover, the shifted peak at 245ºC in NLCs-N DTGA suggested the presence of two peaks which could be attributed to the overlap of Dox and the lipid peaks. Thermal analyses clearly indicated the existence of strong interactions between the lipid components and the Dox, especially for NLCs-N.

The crystalline structure of NLCs and the polymorphism of the lipid matrix were analyzed by XRD **(Figure 1D)**. Drugs have the propensity to exhibit different molecular arrangements in nanocarrier lattices [42]. Analysis of the crystalline structure of Dox and NLCs can help to optimize formulation. Moreover, it has been also reported that crystalline structure of lipids have strong effects on drug EE and controlled release kinetic [43,44]. Fats can crystallize in three main polymorphic forms, in which the α form is unstable, the β is the most stable and the β´ a metastable form, still possesses disorders regions and maintains a partial amorphous state [45].

NLCs showed a mixture of polymorphisms characterized by short spacing (d) obtained from XRD patterns. “d” corresponds to the distance due to lateral packing of the fatty acid chains on the triacylglycerol molecules [46]. NLCs patterns displayed characteristic short spacing at 0.47/0.38/0.37 nm (typical of the β modification) and 0.42/0.38 nm (β´ form) [45]. Dox diffractogram exposed the presence of three peaks (2Θ= 28.47º, 31.81º and 45.58º) suggesting the existence of Dox crystals on its pure form [47]. On the other hand, NLCs diffractogram showed the corresponding peaks to myristyl myristate (2θ= 19.11°, 21.59°, 23.23° and 23.80°), as previously reported [41]. When NLCs were loaded with Dox the XRD patterns exhibited peaks at similar scattered 2Θ angles of 18.66º, 20.94º, 22.75º and 23.50º for NLCs-N and 19.18º, 21.51º, 23.32º and 23.80º for NLCs-H. The fusion of the last two peaks suggests the predominance of β´ architecture in both NLCs. NLCs-N showed a decrease on the intensity of 23.50º peak and an increase on peak at 22.75º. This result indicates partial transition of the NLCs structure from a more stable form (β) to the metastable polymorphism (β´). The more stable the crystal structure, the more organized the molecules will be within the lattice, allowing a better release of the entrapped compounds [46,48]. Thus, the predominance of the metastable polymorphism it is always preferred for sustained drug release.

While morphology, size and surface charge remain almost without changes for both formulations, structural differences were found. Changes on nanostructure suggested that NLCs could work differently as drug delivery systems. At this point, a very simple approach has been developed to produce two chemotherapeutic nanoformulations with different properties and capabilities.

3.2. Drug release from NLCs

Drug release studies were performed to evaluate the capability of NLCs of providing Dox sustained release. **Figure 2** showed the hyperbolic curves for Dox released from NLCs after five days incubation. The dependence of drug release with pH was assayed at pH 7.4 and 5.0 which simulates physiologic environment and the acidic conditions for cell internalization by endocytic pathway respectively [49]. All kinetics showed an initial Dox burst release, followed by a decrease of the drug releasing rate. Significant differences were found between the amount of Dox released from NLCs-H and NLCs-N at both pHs ($p \leq 0.05$). One of the factors affecting the initial burst for NLCs-H was the presence of non-encapsulated Dox in the formulation. NLCs-H showed high release rate reaching the 100% at pH 5.0 and 66% at pH 7.4 after 5 days. In contrast, NLCs-N displayed high capacity to retain Dox and very slow release could be observed. The corresponding drug release kinetic showed to be similar to a zero order profile. After 5 days, 80% to 90% of the total Dox payload was still entrapped into NLCs-N. These differences could be explained by the hydrophilic and hydrophobic nature of each form of Dox. This data agreed with the analysis obtained from XRD patterns. NLCs-H showed high structural stability and therefore more prone to expel the drug. It was also relevant to observe the pH dependence of the release [50]. In both systems, Dox release increased around 1.5 times when pH turn from neutral to acidic values, which is a powerful tool regarding active targeting therapies using tumor-specific pH-responsive nanocarriers [51]. Both NLCs systems provide different Dox release patterns, but NLCs behavior under the tested pHs can be predicted independently of the residual charge of

Dox. As described before, nanoformulations with different release properties allow to being capable to design variable mixtures between both types of NLCs for combinatorial therapy approaches. Here, in a novel approach two Dox nanoformulations were developed with different properties, leaving open the possibility to their use as a combinatorial therapy using the same active principle. This approach could be helping to generate personalized medicine tools where therapy can be customized according to the disease profile of each patient.

3.3 Cell internalization

Images (**Figure 3)** showed that free Dox internalized and quickly concentrated at cell nucleus (co-stained with Hoechst) after 2 h incubation, while Dox fluorescence associated to NLCs-N only appeared in specific zones of the cell cytoplasm, co-stained with Lysotracker green. It is worth mentioning that Dox is a small molecule (Mw= 543.5 g mol^{-1}) and internalizes by simple passive transport (diffusion) [52]. In contrast, molecules of high molecular weight and macromolecular structures (like nanoparticles) are usually internalized by active transport such as endocytosis [53]. Moreover, Dox intercalates between DNA base pairs preventing DNA replication and therefore, its main action takes place within the nucleus [54]. Indeed, images of cells confirmed the presence of free Dox localized within the nucleus, while Dox from NLCs-N were located inside lysosomes.

Subsequently, the molecular state of Dox released from NLCs inside the cell was followed by fluorescence confocal spectral imaging (FCSI). FCSI technique is based on the full fluorescence spectra of Dox measured at different cell points and provides valuable information about the molecular state of the drug once internalized into the cell. Furthermore, analysis on Dox species was focused in the nucleus and in the cytoplasm **(Figure 4)**. Cells were incubated for 1 and 22 h with the nanoparticles. In **Figure 4A** two different spectral profiles are shown, one corresponding to the cytoplasmic region (blue spectrum in **Figure 4A**, blue zone in **Figure 4B** and blue bar in **Figure 4C**) and the other to the nuclear region (red spectrum in **Figure 4A**, red zone in **Figure 4B** and red bar in **Figure 4C**). Dox fluorescence spectra of these two intracellular locations are significantly different from that observed with NLCs-N suspension in PBS (**Figure 4A**, green spectrum and green bars in **Figure 4C**). The cytosolic spectra showed an increase on the left shoulder which is characteristic of Dox fluorescence when the molecule is in low polarity environments like cytosolic membrane-enriched organelles such as endosomes and lysosomes [55,56]. The nuclear Dox spectra were shifted to a high wavelength because of the drug intercalation between base pairs of DNA [55]. In fact, no Dox was found in the nucleus after 1 h incubation of the cells with the NLCs. However, nuclear Dox fluorescence relative fraction significantly increased after 22 h **(**red bar in **Figure 4C**), indicating that Dox was finally released from NCLs accumulated in lysosomes and capable to penetrate the nucleus. The overall intracellular drug fluorescence was also increased.

Cell internalization of NLCs-H and NLC-N was compared also by flow cytometry after 6 h incubation (**Figure S3**). As expected, results showed that NLCs-H internalized much better than NLCs-N, as rate reflected by higher Dox fluorescence values in the former nanoparticles. Overall internalization assays by either confocal microcopy or flow cytometry support the idea that

NCLs-N had been slowly internalized into MDA-MB-231 breast cancer cells, mainly through the endocytic pathway. These results are advantageous for cancer treatment since they exhibited the property of the developed nanoformulation to bypasses the resistance mechanism of cancer cells such as efflux pumps [20].

3.4. *In vitro* efficacy of NLCs

The ability of NLCs loaded with both species of Dox to decrease cell viability was tested using metastatic breast cancer cell line MDA-MB-231. MDA-MB-231 cells correspond to an aggressive, invasive and poorly differentiated human breast cancer cell line with mesenchymal phenotype. Further, MDA-MB-231 is a Dox resistant cell line, meaning that higher doses of the drug are required to kill these cells [57]. The half maximal inhibitory concentration (IC_{50}) of Dox was determined by MTT assays after incubation with free Dox, NLCs-H and NLCs-N at equivalent Dox concentrations (**Figure 5**). The IC_{50} values for free Dox (24.32 ± 1.21 μM) were reduced in NLCs-N (2.17 ± 0.42 μM) and NLC-H (1.28 ± 0.33 μM) indicating that the efficacy of the Dox was improved by the use of nanostructured lipids as drug carriers. Even though cell internalization process was slower for NLCs, the sustained release of the drug in nanostructured lipids increased the efficacy of the free drug. Among both NLCs, the NLCs-H showed better results than NLCs-N after 72 h incubation, probably because NLCs-H internalized faster in cells and showed a quicker drug release profile than NLCs-N. On the other hand, and as expected, unloaded NLCs exhibited no cytotoxicity after 72 h incubation, indicating that the drug carrier was innocuous to the cells at the concentrations equivalent to those used for NLCs-H and NLCs-N.

3.5. NLCs encapsulation into BC matrix

Dox loaded NLCs were entrapped into BC films with the aim of generate a polymeric system for local drug delivery. BC alone was not suitable to entrap small molecules like Dox as previously reported [15,58]. Here, we suggest that the encapsulation of Dox into a hydrophobic nanocarrier followed by the loading into BC films to improve drug's EE and release profile. The procedure involves the immersion of films into free Dox (BC-Dox), NLCs-N (BC-NLCs-N) and mixed NLCs-H/NLCs-N (BC-NLCs-NH) solutions with equivalent Dox concentration of 1.0 mM. Free Dox was encapsulated in low amounts into BC while NLCs increased more than twice Dox EE (**Table 2**). Particularly, NLCs-N generated the highest Dox EE values. The presence of non-encapsulated Dox in NLCs-H formulation could be contributing to lower EE in NLCs mixture. In both cases, it was remarkable that the amount of Dox equivalent payload within NLCs was in the same range than Dox doses administrated in previously reported *in vivo* experiments using free Dox or Dox containing materials [59–61].

Drug's release profiles (**Figure 6)** showed that BC-Dox released almost all its payload during the first 24 h. On the opposite, BC-NLCs-N showed extended and sustained release with only 22% Dox release after two weeks. Dox release from BC-NLCs-NH was 53% in 14 days. Therefore, in the BC-NLCs-NH mixture, NLCs-H exhibited more quickly Dox release, allowing

a strong burst release at initial times, while NLCs-N guaranteed a prolonged and sustained release of the drug. Since both types of NLCs can be mixed at different proportions to modulate release kinetics, there were tested different NLCs ratios to establish proper conditions for *in vivo* Dox dosage. In this case, 80/20 NLCs-H/NLCs-N ratio was established as the best formulation, with a release of the 50% of the payload after 24 h (**Figure 6**). At this point, Dox concentrations reached levels comparable to those previously reported in *in vivo* breast cancer models [62–64]. Moreover, after the first 24 h, the released drug amount was sustained in time.

SEM images showed NLCs entrapped inside the polymeric network and fused to the cellulose fibers **(Figure 7A & 7B)**. Additionally, TEM observations of the supernatants from release assays were performed to verify the presence of nanoparticles. Images showed NLCs released from the BC matrix with conserved spherical morphology (**Figure 7C & 7D**). The novel nanoparticle-hydrogel matrix showed the excellence of integrating a bacterial cellulose network and a lipid nanoformulation in a platform easy to produce and handle. In one hand, BC was obtained by a simple and environmentally friendly process, and has a very high biocompatibility. On the other hand, NLCs formulation showed therapeutic advantages in comparison with free Dox, envisioning a potential synergism with the combined use of BC and NLC in vivo.

3.6. *In vivo* antitumor efficacy and tolerability of BC-NLCs-NH films

The use of nanomaterials as drug releasing platforms for localized treatment of tumors has long attracted the attention of research scientists [59,61], as a way to control tumor growth or local relapses in unresectable tumors and resectable tumors, respectively. To determine the efficacy and tolerability of BC-NLCs-NH films, MDA-MB-231 cells were implanted i.m.f.p. into nude mice and 16 days post-tumor inoculation, 0.14 mg Dox equivalent/mouse treatment was applied by BC-NLCs-NH implantation or intratumoral administration of free Dox. Since the objective of the study was to determine the advantages of using BC-NLCs-NH hybrid system in the local treatment of tumors, we did not include any systemic treatment with Dox, whose toxicities and tumor inhibiting capabilities have been widely described in the literature [54,59,60,65,66]. Plain BC was not considered as a control group either because its biocompatibility has been well-reported previously [67–70]. Indeed, as a preparatory training exercise, before implanting Dox loaded matrices into immunodeficient mice, we also tested the implantation of circular matrices (∅= 12 mm) subcutaneously in the rear flank of immunocompetent C57Bl6 mice (n=3). One week after implantation, animals showed no weight loss or distress symptoms, nor there were locals signs of inflammation, necrosis or cellular atypia.

Figure 8A shows the comparative analysis of the antitumoral activity of BC-NLCs-NH and free Dox determined as tumor volume *in vivo*. Both, BC-NLCs-NH and free Dox induced a significant delay in tumor growth compared to non-treated controls. Importantly, BC-NLCs-NH could reach free Dox range of tumor response. At 36 days after treatment initiation, animals were euthanized and primary tumors were removed (**Figure 8B**). *In vivo*, at the time of euthanasia, tumor volumes in BC-NLCs-NH treated mice were significantly smaller than in non-treated animals (t Student, p=0.0025), being this difference higher than in the free Dox group (t Student, p=0.0082). *Ex vivo,* tumor volume values confirmed the above results, showing smaller tumors for BC-NLCs-NH

treated mice (t Student vs. control, p=0.0061), compared to those with intratumoral administration of free Dox (t Student vs. control, p=0.0123). Indeed, Tumor to control (T/C) ratios of tumor volume *ex vivo* for BC-NLCs-NH and free Dox were 53% and 66%, respectively, whereas tumor weight *ex vivo* was 62% and 81%, respectively.

Although these treatments were thought for a localized treatment of primary tumors, it is also interesting to evaluate the effect of the treatments in the metastatic process, because inhibition of the primary tumor growth by these type of treatments might well reduce the large number of cells that primary tumors are continuously shedding to the circulation [71,72]. In our case, metastatic lesions at the mammary chain (loco-regional dissemination), lumbar lymph nodes (lymphatic dissemination) and lung (hematologic dissemination) were detected only in non-treated control mice (Sup. Table 1), indicating that BC-NLCs-NH was effective inhibiting the metastatic process by controlling the growth of the primary tumor.

Besides antitumoral activity, toxicity was also determined by monitoring the animal's body weight (T/C ratio), eating and physical activity parameters. Body weight of the animals treated with BC-NLCs-NH and free Dox was maintained along the treatment time and no changes in eating, drinking, grooming, exploratory behavior, activity, and neurological status were observed. However, for free Dox treated animals, inflammation at the tumor site was observed the first 20 days after treatment (38% of the animals), and tumor external necrosis was induced (63% of the animals) (Table 3). On the contrary, implantation of BC-NLCs-NH system into tumor site did not induce inflammation or external tumor necrosis in any case. Moreover, heart weight was also studied to examine Dox-associated toxicities, as previously observed after repeated systemic administrations of Dox [54,59]. Intratumoral Dox administration or tumor implantation of the films prevented Dox release at high doses to systemic circulation, avoiding such toxicities. Thus, BC-NLCs-NH reached free Dox range tumor response while diminishing Dox-related toxicities.

To the best of our knowledge, the potentiality of bacterial cellulose as hydrogel for local cancer therapy was never reported nor it was tested the combination of bacterial cellulose matrix with lipidic nanocarriers *in vivo*. Overall, our results show that the therapeutic index of Dox can be improved when the drug, locally administrated, is entrapped inside a polymeric matrix and released in a sustained way. It has been already reported that prolonged exposure of low-dose chemotherapy is clinically beneficial [73,74] as it might happen with BC-NLCs-NH. Indeed, a potential limitation of the current study is that since animals were euthanized before BC-NLCs-NH could release all its content, the therapeutic potential of the BC-NLCs-NH in terms of increased efficacy has not been completely exploited. However, moved by the positive results in terms of safety of the initial BC-NLCs-NH system, we are currently evaluating different ways to increase the antitumor effect of the BC matrix. One of the strategies employed in this optimization process includes the functionalization of NLCs with targeting molecules that facilitate cell internalization.

4. CONCLUSIONS

In summary, we here present a novel hydrogel-nanoparticle hybrid system for localized cancer treatment, combining the use of bacterial cellulose matrix with lipidic nanocarriers (NLCs). To the best of our knowledge this is the first work describing the use of bacterial cellulose as an implantable matrix for local chemotherapy in cancer.

We demonstrated that NLCs loaded with cationic or neutral forms of Dox exhibited different release profiles and that the integration of both NLCs systems in a unique formulation allowed combining both release kinetics for a more efficient drug exposition. *In vitro* experiments established that NLCs are internalized into cells by the endocytic pathway, leading to potentially overcome MDR mechanisms, while the sustained release of the drug from nanostructured particles allowed an increased efficacy over the free Dox. Based on these *in vitro* results, a drug delivery device with a mixed NLCs formulation loaded into BC membranes (BC-NLCS-NH) was designed and tested *in vivo* in an orthotopic breast cancer tumor model. Tumors treated with BC-NLCs-NH showed a very significant tumor growth delay, even better than the intratumorally administered Dox, but without the side effects such as edema, inflammation and necrosis observed in free-Dox treated mice.

In short, our experimental evidences confirmed that BC-NLCs-NH hydrogel-nanoparticle hybrid system could be easily implanted for local treatment of tumors as a neo-adjuvant therapy. As a device, this hybrid system facilitates the delivery and accumulation of chemotherapeutic nanoparticles into the tumor site, promoting the efficacy of released drug against cancer cells and reducing therapeutic undesirable side effects of the free drugs.

Conflicts of interest

There are no conflicts to declare.

Acknowledgements

We acknowledge financial support by Argentinian grants from the National Council for Science and Technology (CONICET, PIP 0498) and the National Agency of Scientific and Technological Promotion (ANPCyT, PICT 2016-4597) to GRC. From the Spanish side, this work was supported by *Instituto de Salud* Carlos III, through Networking Research Center on Bioengineering, Biomaterials, and Nanomedicine (CIBER-BBN) an initiative that also counts with the assistance from the European Regional Development Fund; and by the "*Fundació Marató* TV3" (337/C/2013) to IA. The Argentinian Ministry of Science, Technology and Innovative Production supported MLC stance at FVPR through the BecAR internship program. Finally, the Spanish Ministry of Science and Innovation supported NG-A as laboratory technician (PTA2013-8431-I). Additionally, we acknowledge the ICTS"NANBIOSIS, more specifically the CIBER-BBN's *in vivo* Experimental Platform at the Functional Validation & Preclinical Research (FVPR) area

(www.nanbiosis.es/unit/860 u20-in-vivo-experimental-platform). We are also grateful to Laia Foradada Felip for her contribution to the design and performance of *in vivo* assays. Finally, we would like to thanks LKM pharmaceuticals (Argentina) for kindly supplying Doxorubicin hydrochloride.

References

[1] L.A. Torre, F. Bray, R.L. Siegel, J. Ferlay, J. Lortet-tieulent, A. Jemal, Global Cancer Statistics, 2012, CA a Cancer J. Clin. 65 (2015) 87–108. doi:10.3322/caac.21262.

[2] J.B. Wolinsky, Y.L. Colson, M.W. Grinstaff, Local drug delivery strategies for cancer treatment: Gels, nanoparticles, polymeric films, rods, and wafers, J. Control. Release. 159 (2012) 14–26. doi:10.1016/j.jconrel.2011.11.031.

[3] A. Fakhari, J. Anand Subramony, Engineered in-situ depot-forming hydrogels for intratumoral drug delivery, J. Control. Release. 220 (2015) 465–475. doi:10.1016/j.jconrel.2015.11.014.

[4] A.I. Minchinton, I.F. Tannock, Drug penetration in solid tumours., Nat. Rev. Cancer. 6 (2006) 583–592. doi:10.1038/nrc1893.

[5] S.H. Jang, M.G. Wientjes, D. Lu, J.L.S. Au, Drug delivery and transport to solid tumors, Pharm. Res. 20 (2003) 1337–1350. doi:10.1023/A:1025785505977.

[6] V.T.J. DeVita, T.S. Lawrence, S.A. Rosenberg, Devita, Hellman, and Rosenberg's cancer : principles & practice of oncology, 10th editi, Philadelphia : Wolters Kluwer, [2015], Philadelphia, EEUU, 2015.

[7] P.E. Saw, J. Park, S. Jon, O.C. Farokhzad, A drug-delivery strategy for overcoming drug resistance in breast cancer through targeting of oncofetal fibronectin, Nanomedicine Nanotechnology, Biol. Med. 13 (2016) 713–722. doi:10.1016/j.nano.2016.10.005.

[8] C. Holohan, S. Van Schaeybroeck, D.B. Longley, P.G. Johnston, Cancer drug resistance: an evolving paradigm, Nat. Rev. Cancer. 13 (2013) 714–726. doi:10.1038/nrc3599.

[9] I.A. Khawar, J.H. Kim, H.J. Kuh, Improving drug delivery to solid tumors: Priming the tumor microenvironment, J. Control. Release. 201 (2015) 78–89. doi:10.1016/j.jconrel.2014.12.018.

[10] L.K. Fung, W.M. Saltzman, Polymeric implants for cancer chemotherapy, Adv. Drug Deliv. Rev. 26 (1997) 209–230. doi:10.1016/S0169-409X(97)00036-7.

[11] R. De Souza, P. Zahedi, C.J. Allen, M. Piquette-Miller, Polymeric drug delivery systems for localized cancer chemotherapy., Drug Deliv. 17 (2010) 365–375. doi:10.3109/10717541003762854.

[12] W. Gao, Y. Zhang, Q. Zhang, L. Zhang, Nanoparticle-Hydrogel: A Hybrid Biomaterial System for Localized Drug Delivery, Ann. Biomed. Eng. 44 (2016) 2049–2061. doi:10.1007/s10439-016-1583-9.

[13] E.S. Place, N.D. Evans, M.M. Stevens, Complexity in biomaterials for tissue engineering, Nat. Mater. 8 (2009) 457–470. doi:10.1017/CBO9781107415324.004.

[14] M.M. Abeer, M.C.I. Mohd Amin, C. Martin, A review of bacterial cellulose-based drug delivery systems: Their biochemistry, current approaches and future prospects, J. Pharm. Pharmacol. 66 (2014) 1047–1061. doi:10.1111/jphp.12234.

[15] M.L. Cacicedo, I. E. León, J. S. Gonzalez, L. M. Porto, V. A. Alvarez, G.R. Castro,

Modified bacterial cellulose scaffolds for localized doxorubicin release in human colorectal HT-29 cells, Colloids Surf. B Biointerfaces. 140 (2016) 421–429. doi:10.1016/j.colsurfb.2016.01.007.

[16] M.L. Cacicedo, M.C. Castro, I. Servetas, L. Bosnea, K. Boura, P. Tsafrakidou, A. Dima, A. Terpou, A. Koutinas, G.R. Castro, Progress in bacterial cellulose matrices for biotechnological applications, Bioresour. Technol. 213 (2016) 172–180. doi:10.1016/j.biortech.2016.02.071.

[17] FDA, C. for D.E. and Research, Guidances (Drugs)—Guidance for Industry: Pyrogenand Endotoxins Testing: Questions and Answers, (2016). http://www.fda.gov/Drugs/GuidanceComplianceRegulatoryInformation/Guidances/ucm314718.htm (accessed February 12, 2016).

[18] J. Shi, A.R. Votruba, O.C. Farokhzad, R. Langer, Nanotechnology in drug delivery and tissue engineering: From discovery to applications, Nano Lett. 10 (2010) 3223–3230. doi:10.1021/nl102184c.

[19] M. Sethi, R. Sukumar, S. Karve, M.E. Werner, E.C. Wang, D.T. Moore, S.R. Kowalczyk, L. Zhang, A.Z. Wang, Effect of drug release kinetics on nanoparticle therapeutic efficacy and toxicity., Nanoscale. 6 (2014) 2321–7. doi:10.1039/c3nr05961h.

[20] H. Meng, W. Mai, H. Zhang, M. Xue, T. Xia, S. Lin, X. Wang, Y. Zhao, Z. Ji, J. Zink, A. Nel, Codelivery of an optimal drug/siRNA combination Using Mesoporous Silica Nanoparticles To Overcome Drug Resistance in Breast Cancer in Vitro and in Vivo, ACS Nano. 7 (2013) 994–1005. doi:10.1021/nn3044066.

[21] M. Creixell, N.A. Peppas, Co-delivery of siRNA and therapeutic agents using nanocarriers to overcome cancer resistance, Nano Today. 7 (2012) 367–379. doi:10.1016/j.nantod.2012.06.013.

[22] D. Liu, Z. Liu, L. Wang, C. Zhang, N. Zhang, Nanostructured lipid carriers as novel carrier for parenteral delivery of docetaxel, Colloids Surfaces B Biointerfaces. 85 (2011) 262–269. doi:10.1016/j.colsurfb.2011.02.038.

[23] S. Das, W.K. Ng, R.B.H. Tan, Are nanostructured lipid carriers (NLCs) better than solid lipid nanoparticles (SLNs): Development, characterizations and comparative evaluations of clotrimazole-loaded SLNs and NLCs?, Eur. J. Pharm. Sci. 47 (2012) 139–151. doi:10.1016/j.ejps.2012.05.010.

[24] G. Chen, K. Wang, Y. Zhou, L. Ding, A. Ullah, Q. Hu, M. Sun, D. Oupický, Oral Nanostructured Lipid Carriers Loaded with Near-Infrared Dye for Image-Guided Photothermal Therapy, ACS Appl. Mater. Interfaces. (2016) acsami.6b07425. doi:10.1021/acsami.6b07425.

[25] Q. Liu, J. Li, G. Pu, F. Zhang, H. Liu, Y. Zhang, Co-delivery of baicalein and doxorubicin by hyaluronic acid decorated nanostructured lipid carriers for breast cancer therapy, Drug Deliv. 00 (2015) 1–5. doi:10.3109/10717544.2015.1031295.

[26] X. Dong, W. Wang, H. Qu, D. Han, J. Zheng, G. Sun, Targeted delivery of doxorubicin and vincristine to lymph cancer: evaluation of novel nanostructured lipid carriers in vitro and in vivo., Drug Deliv. 00 (2015) 1–5. doi:10.3109/10717544.2015.1041580.

[27] H. Di, H. Wu, Y. Gao, W. Li, D. Zou, C. Dong, Doxorubicin- and cisplatin-loaded nanostructured lipid carriers for breast cancer combination chemotherapy, Drug Dev. Ind. Pharm. 42 (2016) 2038–2043. doi:10.1080/03639045.2016.1190743.

[28] M.S. Oliveira, B. Aryasomayajula, B. Pattni, S. V. Mussi, L.A.M. Ferreira, V.P. Torchilin, Solid lipid nanoparticles co-loaded with doxorubicin and ??-tocopherol succinate are effective against drug-resistant cancer cells in monolayer and 3-D spheroid cancer cell models, Int. J. Pharm. 512 (2016) 292–300. doi:10.1016/j.ijpharm.2016.08.049.

[29] P. Ma, X. Dong, C.L. Swadley, A. Gupte, M. Leggas, H.C. Ledebur, R.J. Mumper, Development of idarubicin and doxorubicin solid lipid nanoparticles to overcome Pgp-mediated multiple drug resistance in leukemia, J. Biomed. Nanotechnol. 5 (2009) 151–161. doi:10.1166/jbn.2009.1021.

[30] K. Bogman, F. Erne-Brand, J. Alsenz, J. Drewe, The role of surfactants in the reversal of active transport mediated by multidrug resistance proteins, J. Pharm. Sci. 92 (2003) 1250–1261. doi:10.1002/jps.10395.

[31] M.C. Cavaco, C. Pereira, B. Kreutzer, L.F. Gouveia, B. Silva-Lima, A.M. Brito, M. Videira, Evading P-glycoprotein mediated-efflux chemoresistance using Solid Lipid Nanoparticles, Eur. J. Pharm. Biopharm. 110 (2017) 76–84. doi:10.1016/j.ejpb.2016.10.024.

[32] M. Chu, H. Gao, S. Liu, L. Wang, Y. Jia, M. Gao, M. Wan, C. Xu, L. Ren, Functionalization of composite bacterial cellulose with C 60 nanoparticles for wound dressing and cancer therapy †, RSC Adv. 8 (2018) 18197–18203. doi:10.1039/C8RA03965H.

[33] V. Venkateswarlu, K. Manjunath, Preparation, characterization and in vitro release kinetics of clozapine solid lipid nanoparticles, J. Control. Release. 95 (2004) 627–638. doi:10.1016/j.jconrel.2004.01.005.

[34] J.B. Chaires, N. Dattagupta, D.M. Crothers, Self-Association of Daunomycin, Biochemistry. (1982) 3927–3932.

[35] Z. Fülöp, R. Gref, T. Loftsson, A permeation method for detection of self-aggregation of doxorubicin in aqueous environment, Int. J. Pharm. 454 (2013) 559–561. doi:10.1016/j.ijpharm.2013.06.058.

[36] T. Mosmann, Rapid colorimetric assay for cellular growth and survival: Application to proliferation and cytotoxicity assays, J. Immunol. Methods. 65 (1983) 55–63. doi:10.1016/0022-1759(83)90303-4.

[37] E. Perillo, E. Allard-Vannier, A. Falanga, P. Stiuso, M.T. Vitiello, M. Galdiero, S. Galdiero, I. Chourpa, Quantitative and qualitative effect of gH625 on the nanoliposome-mediated delivery of mitoxantrone anticancer drug to HeLa cells, Int. J. Pharm. 488 (2015) 59–66. doi:10.1016/j.ijpharm.2015.04.039.

[38] M. Ahmadi, T. Madrakian, A. Afkhami, Solid phase extraction of doxorubicin using molecularly imprinted polymer coated magnetite nanospheres prior to its spectrofluorometric determination, New J. Chem. 39 (2015) 163–171. doi:10.1039/C4NJ01402B.

[39] R.J. Sturgeon, S.G. Schulman, Electronic absorption spectra and protolytic equilibria of doxorubicin: Direct spectrophotometric determination of microconstants, J. Pharm. Sci. 66 (1977) 958–961. doi:10.1002/jps.2600660714.

[40] C. He, Y. Hu, L. Yin, C. Tang, C. Yin, Effects of particle size and surface charge on cellular uptake and biodistribution of polymeric nanoparticles, Biomaterials. 31 (2010) 3657–3666. doi:10.1016/j.biomaterials.2010.01.065.

[41] G.A. Islan, P.C. Tornello, G.A. Abraham, N. Duran, G.R. Castro, Smart lipid nanoparticles containing levofloxacin and DNase for lung delivery. Design and characterization, Colloids Surf. B Biointerfaces. 143 (2016) 168–176. doi:10.1016/j.colsurfb.2016.03.040.

[42] B. Rodenak-Kladniew, G.A. Islan, M.G. de Bravo, N. Durán, G.R. Castro, Design, characterization and in vitro evaluation of linalool-loaded solid lipid nanoparticles as potent tool in cancer therapy, Colloids Surf. B Biointerfaces. 154 (2017) 123–132. doi:10.1016/j.colsurfb.2017.03.021.

[43] A. Tupal, M. Sabzichi, F. Ramezani, M. Kouhsoltani, H. Hamishehkar, Dermal delivery of doxorubicin-loaded solid lipid nanoparticles for the treatment of skin cancer, J. Microencapsul. 2048 (2016) 1–9. doi:10.1080/02652048.2016.1200150.

[44] Y. Da Dong, B.J. Boyd, Applications of X-ray scattering in pharmaceutical science, Int. J. Pharm. 417 (2011) 101–111. doi:10.1016/j.ijpharm.2011.01.022.

[45] H. Bunjes, T. Unruh, Characterization of lipid nanoparticles by differential scanning calorimetry, X-ray and neutron scattering, Adv. Drug Deliv. Rev. 59 (2007) 379–402. doi:10.1016/j.addr.2007.04.013.

[46] J. Yang, O.N. Ciftci, Formation of hollow solid lipid micro- and nanoparticles using supercritical carbon dioxide, Food Bioprod. Process. 98 (2016) 151–160. doi:10.1016/j.fbp.2016.01.004.

[47] A. Margaritis, B. Manocha, Controlled release of doxorubicin from doxorubicin/??-polyglutamic acid ionic complex, J. Nanomater. 2010 (2010). doi:10.1155/2010/780171.

[48] P.J. Lawler, P.S. Dimick, Crystallization and polymorphismof fats, in: C.C. Akoh, D.B. Min (Eds.), Food Lipids Chem. Biotechnol., CRC Press, Boca Raton, FL, 2008: p. 253. doi:http://dx.doi.org/10.1201/9781420046649.ch9.

[49] N. Oh, J.H. Park, Endocytosis and exocytosis of nanoparticles in mammalian cells, Int. J. Nanomedicine. 9 (2014) 51–63. doi:10.2147/IJN.S26592.

[50] S.V. Mussi, R.C. Silva, M.C. De Oliveira, C.M. Lucci, R.B. De Azevedo, L.A.M. Ferreira, New approach to improve encapsulation and antitumor activity of doxorubicin loaded in solid lipid nanoparticles, Eur. J. Pharm. Sci. 48 (2013) 282–290. doi:10.1016/j.ejps.2012.10.025.

[51] Y. Zhao, W. Ren, T. Zhong, S. Zhang, D. Huang, Y. Guo, X. Yao, C. Wang, W.Q. Zhang, X. Zhang, Q. Zhang, Tumor-specific pH-responsive peptide-modified pH-sensitive liposomes containing doxorubicin for enhancing glioma targeting and anti-tumor activity, J. Control. Release. 222 (2016) 56–66. doi:10.1016/j.jconrel.2015.12.006.

[52] J. Gautier, E. Munnier, M. Souc??, I. Chourpa, L. Douziech Eyrolles, Analysis of doxorubicin distribution in MCF-7 cells treated with drug-loaded nanoparticles by combination of two fluorescence-based techniques, confocal spectral imaging and capillary electrophoresis, Anal. Bioanal. Chem. (2015) 3425–3435. doi:10.1007/s00216-015-8566-9.

[53] M. Mahmoudi, K. Azadmanesh, M.A. Shokrgozar, W.S. Journeay, S. Laurent, Effect of nanoparticles on the cell life cycle, Chem. Rev. 111 (2011) 3407–3432. doi:10.1021/cr1003166.

[54] K.R. Hande, Topoisomerase II inhibitors, Update Cancer Ther. 3 (2008) 13–26. doi:10.1016/j.uct.2008.02.001.

[55] J. Gautier, E. Munnier, A. Paillard, K. Hervé, L. Douziech-Eyrolles, M. Soucé, P. Dubois, I. Chourpa, A pharmaceutical study of doxorubicin-loaded PEGylated nanoparticles for magnetic drug targeting, Int. J. Pharm. 423 (2012) 16–25. doi:10.1016/j.ijpharm.2011.06.010.

[56] J. Gautier, E. Munnier, M. Soucé, I. Chourpa, L. Douziech Eyrolles, Analysis of doxorubicin distribution in MCF-7 cells treated with drug-loaded nanoparticles by combination of two fluorescence-based techniques, confocal spectral imaging and capillary electrophoresis, Anal. Bioanal. Chem. 407 (2015) 3425–3435. doi:10.1007/s00216-015-8566-9.

[57] A. Wu, K. Loutherback, G. Lambert, L. Estévez-Salmerón, T.D. Tlsty, R.H. Austin, J.C. Sturm, Cell motility and drug gradients in the emergence of resistance to chemotherapy, Proc. Natl. Acad. Sci. 110 (2013) 16103–16108. doi:10.1073/pnas.1314385110.

[58] M.L. Cacicedo, K. Cesca, V.E. Bosio, L.M. Porto, G.R. Castro, Self-assembly of carrageenin-CaCO3 hybrid microparticles on bacterial cellulose films for doxorubicin sustained delivery, J. Appl. Biomed. 13 (2015) 239–248. doi:10.1016/j.jab.2015.03.004.

[59] F.P. Seib, D.L. Kaplan, Doxorubicin-loaded silk films: Drug-silk interactions and in vivo performance in human orthotopic breast cancer, Biomaterials. 33 (2012) 8442–8450. doi:10.1016/j.biomaterials.2012.08.004.

[60] I. Tekedereli, S.N. Alpay, U. Akar, E. Yuca, C. Ayugo-Rodriguez, H.-D. Han, A.K. Sood, G. Lopez-Berestein, B. Ozpolat, Therapeutic Silencing of Bcl-2 by Systemically Administered siRNA Nanotherapeutics Inhibits Tumor Growth by Autophagy and Apoptosis and Enhances the Efficacy of Chemotherapy in Orthotopic Xenograft Models of ER (-) and ER (+) Breast Cancer., Mol. Ther. Nucleic Acids. 2 (2013) e121. doi:10.1038/mtna.2013.45.

[61] S. Cai, S. Thati, T.R. Bagby, H.M. Diab, N.M. Davies, M.S. Cohen, M.L. Forrest M. Laird, Localized doxorubicin chemotherapy with a biopolymeric nanocarrier improves survival and reduces toxicity in xenografts of human breast cancer, J. Control. Release. 146 (2010) 212–218. doi:10.1016/j.jconrel.2010.04.006.

[62] E.M. Mastria, M. Chen, J.R. McDaniel, X. Li, J. Hyun, M.W. Dewhirst, A. Chilkoti, Doxorubicin-conjugated polypeptide nanoparticles inhibit metastasis in two murine models of carcinoma, J. Control. Release. 208 (2015) 52–58. doi:10.1016/j.jconrel.2015.01.033.

[63] bennett Elzey, S. Torregrosa-Allen, P. Li, B. Ramsey, G. Burcham, M. (Shaw S.L. Shaw, A totally absorbable multilayer PLGA implant device containing doxorubicin inhibited tumor growth and metastasis without systemic toxicity in murine breast cancer and an ideal pharmacological paradigm for regional chemotherapy, J. Biosci. Med. 4 (2016) 66–81. doi:10.4236/jbm.2016.47008.

[64] Y. Du, W. Ren, Y. Li, Q. Zhang, L. Zeng, C. Chi, A. Wu, J. Tian, The enhanced chemotherapeutic effects of doxorubicin loaded PEG coated TiO_2 nanocarriers in an orthotopic breast tumor bearing mouse model, J. Mater. Chem. B. 3 (2015) 1518–1528. doi:10.1039/C4TB01781A.

[65] A. Bandyopadhyay, L. Wang, J. Agyin, Y. Tang, S. Lin, I.T. Yeh, K. De, L.Z. Sun, Doxorubicin in combination with a small TGFβ inhibitor: A potential novel therapy for metastatic breast cancer in mouse models, PLoS One. 5 (2010). doi:10.1371/journal.pone.0010365.

[66] B. Jiang, L. Zhang, Y. Wang, M. Li, W. Wu, S. Guan, X. Liu, M. Yang, J. Wang, D. an Guo, Tanshinone IIA sodium sulfonate protects against cardiotoxicity induced by doxorubicin in vitro and in vivo, Food Chem. Toxicol. 47 (2009) 1538–1544. doi:10.1016/j.fct.2009.03.038.

[67] G.F. Picheth, C.L. Pirich, M.R. Sierakowski, M.A. Woehl, C.N. Sakakibara, C.F. de Souza, A.A. Martin, R. da Silva, R.A. de Freitas, Bacterial cellulose in biomedical applications: A review, Int. J. Biol. Macromol. 104 (2017) 97–106. doi:10.1016/j.ijbiomac.2017.05.171.

[68] J. V. Kumbhar, S.H. Jadhav, D.S. Bodas, A. Barhanpurkar-Naik, M.R. Wani, K.M. Paknikar, J.M. Rrajwade, In vitro and in vivo studies of a novel bacterial cellulose-based acellular bilayer nanocomposite scaffold for the repair of osteochondral defects, Int. J. Nanomedicine. 12 (2017) 6437–6459. doi:10.2147/IJN.S137361.

[69] G. Helenius, H. Bäckdahl, A. Bodin, U. Nannmark, P. Gatenholm, B. Risberg, In vivo biocompatibility of bacterial cellulose, J. Biomed. Mater. Res. - Part A. 76 (2006) 431–438. doi:10.1002/jbm.a.30570.

[70] D.A. Schumann, J. Wippermann, D.O. Klemm, F. Kramer, D. Koth, H. Kosmehl, T. Wahlers, S. Salehi-Gelani, Artificial vascular implants from bacterial cellulose: Preliminary results of small arterial substitutes, Cellulose. 16 (2009) 877–885. doi:10.1007/s10570-008-9264-y.

[71] G.P. Gupta, J. Massagué, Cancer Metastasis: Building a Framework, Cell. 127 (2006) 679–695. doi:10.1016/j.cell.2006.11.001.

[72] T. Frenzel, C. Siekmann, Jordana Grohmann, U. Valentiner, R. Schmitz, K. Riecken, B. Fehse, U. Schumacher, T. Lange, A. Krüll, Locally Ablative Radiation Therapy of a Primary Human Small Cell Lung Cancer Tumor Decreases the Number of Spontaneous Metastases in Two Xenograft Models, Int. J. Radiat. Oncol. 100 (2018) 1044–1056.

[73] P. Zahedi, R. De Souza, M. Piquette-Miller, C. Allen, Chitosan-phospholipid blend for sustained and localized delivery of docetaxel to the peritoneal cavity, Int. J. Pharm. 377 (2009) 76–84. doi:10.1016/j.ijpharm.2009.05.003.

[74] V. Vassileva, J. Grant, R. De Souza, C. Allen, M. Piquette-Miller, Novel biocompatible intraperitoneal drug delivery system increases tolerability and therapeutic efficacy of paclitaxel in a human ovarian cancer xenograft model, Cancer Chemother. Pharmacol. 60 (2007) 907–914. doi:10.1007/s00280-007-0449-0.

Figures captions

Figure 1. **TEM, thermogravimetric and XRD analysis of NLCs**. TEM images were taken at 60,000x from NLCs-N (A) and NLCs-H (B). DTGA curves from the TGA analysis (C) and XRD patterns (D) of pure Dox, NLCs, NLCs-H and NLCs-N were also studied.

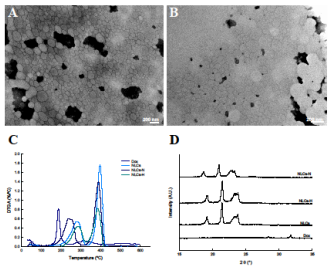

Figure 2. Dox released from the NLCs. Drug released was studied at pH 7.4 (10 mM PBS buffer) and 5.0 (10 mM acetate buffer) (○ NLCs-N, pH 5.0; ● NLCs-N, pH 7.4; Δ NLCs-H, pH 5.0; ▼ NLCs-H, pH 5.0). The results are the mean of two individual experiments, each one performed in duplicate, and the errors were calculated by standard deviation.

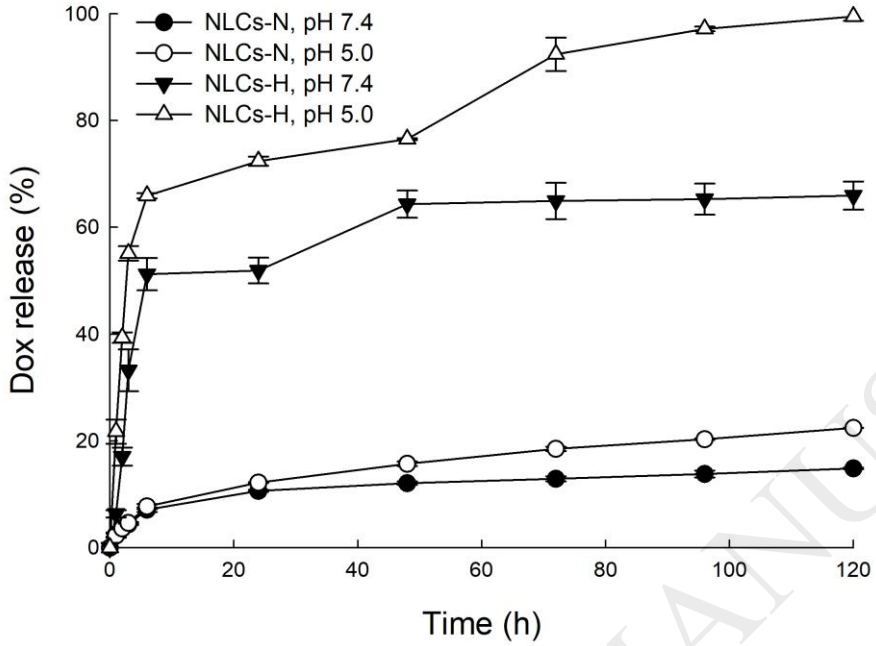

Figure 3. Internalization of NLCs-N in MDA-MB-231 cells. Confocal images of Dox and NLCs-N show that free Dox rapidly reaches the nuclei of cells co-stained with Hoechst, whereas NLCs-N internalize through the endocytic pathways as shown by the co-localization of the Dox signal with the lysosomes (co-stained with Lysotracker green and shown with arrows). Magnification bars corresponds to 10 μm and applies to all images.

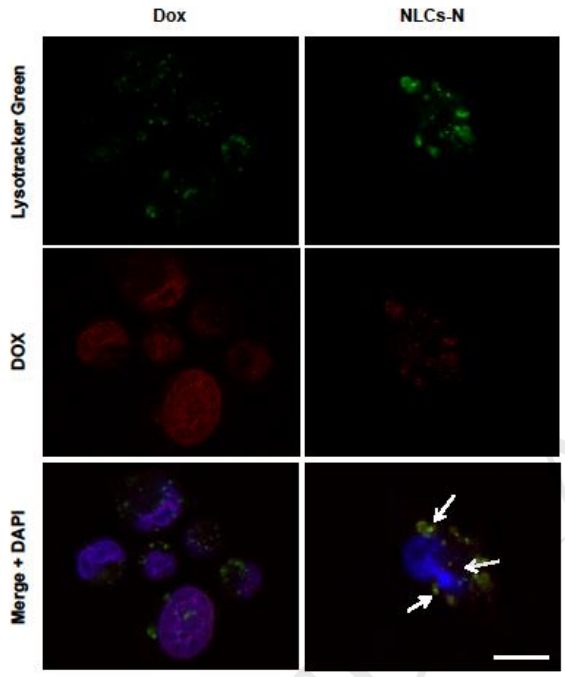

Figure 4. FCSI studies showing the molecular state of Dox delivered by NLCs-N. (A) Characteristic of fluorescence spectra of Dox in initial NLCs-N suspension in PBS (green), in cellular nucleus (red) and cytosol (blue). (B) Examples of subcellular distribution of the Dox fluorescence in MDA-MB-231 cancer cells after 1 or 22 h incubation with NLCs-N. Dashed lines show the nucleus limits. (C) Quantitation of the intracellular Dox fluorescence as averaged from several spectral maps (n= 10) at 1 or 22 h incubation.

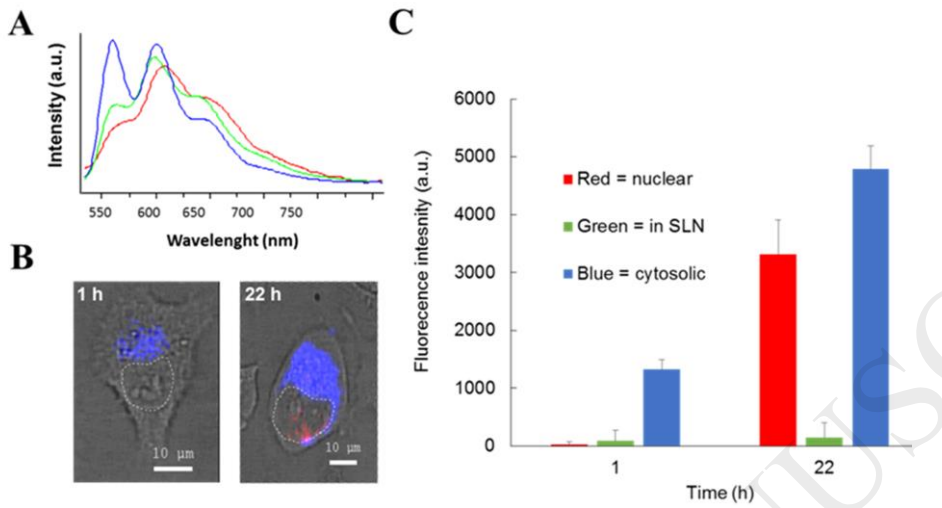

Figure 5. ***In vitro*** **efficacy of Dox loaded NLCs**. Cytotoxicity of free Dox, NLCs-H and NLCs-N after 72 h incubation was measured by MTT. Results are the mean of three independent experiments, and error estimated by standard error of the mean.

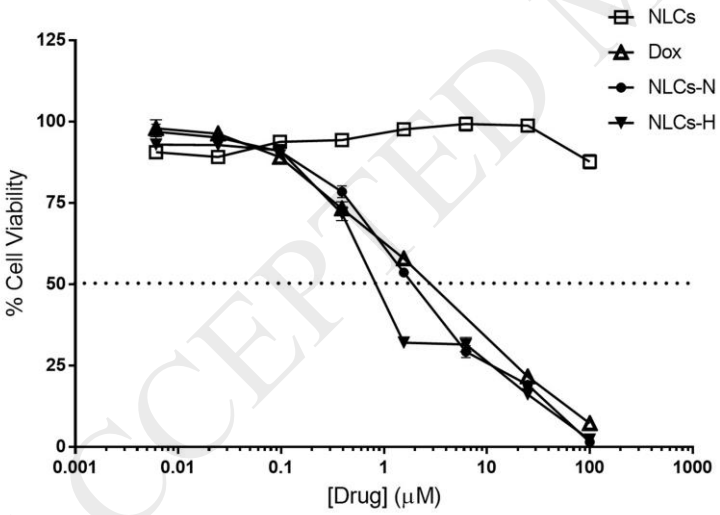

Figure 6. Dox released from drug or NLCs loaded BC films. Release studies were performed at pH 7.4 and 37ºC in PBS. Results correspond to the mean between three individual experiments, each performed in duplicate, and error was calculated by standard deviation.

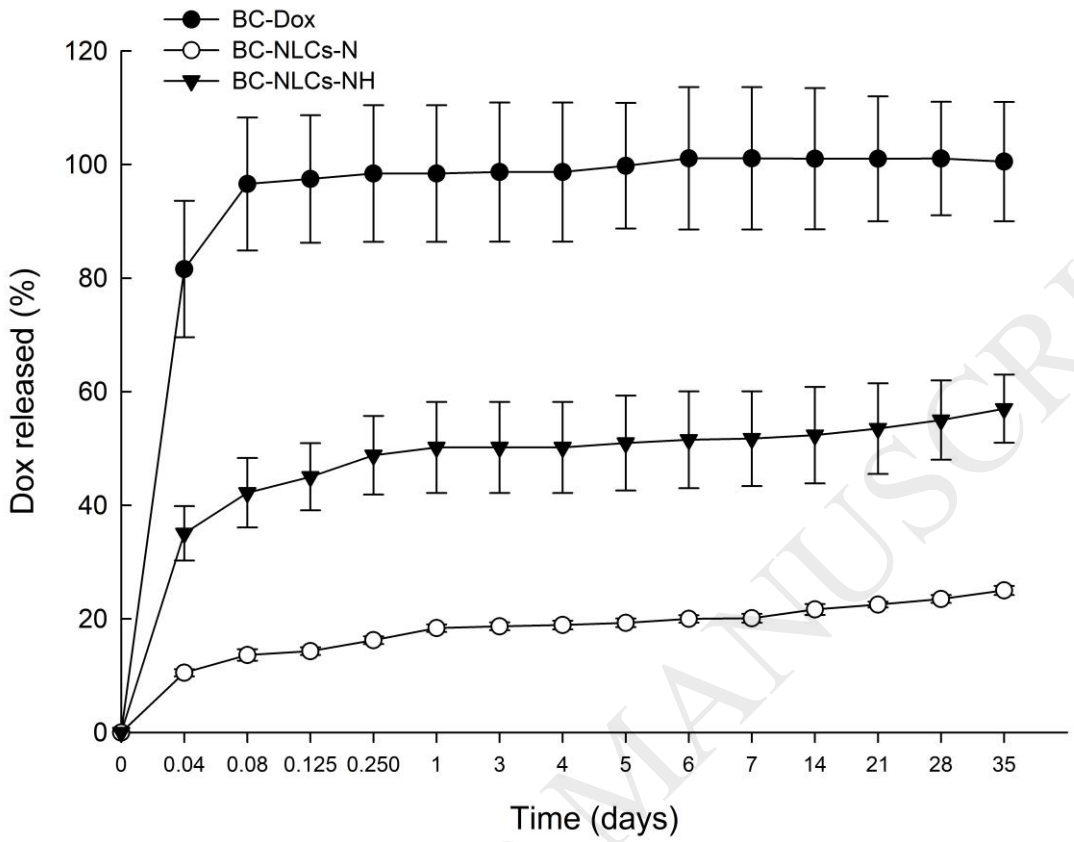

Figure 7. Microscopy studies for BC-NLCs-NH. SEM images were taken at 5,000x (A) and 10,000x (B). TEM images from BC-NLCs-NH supernatant at 50,000x (C) and 100,000x (D).

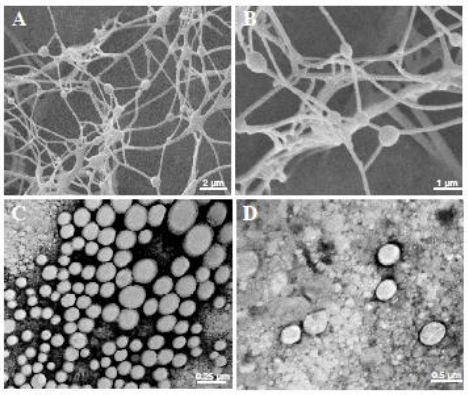

Figure 8. Tumor growth delay induced by BC-NLCs-NH. Comparative analysis of the localized i.m.f.p. growth of the MDA-MB-231 BCa cells treated locally with a BC film loaded with a mix of NLCs-N:NLCs-H (20:80) (BC-NLCs-NH) containing 0.14 mg of Dox or free Dox (0.14 mg as a unique dose given intratumoraly) in athymic nude mice. (A) Conventional measurements of tumor volume over time, and (B) individual tumor volu me at end point along with representative tumor photographs *ex vivo*.

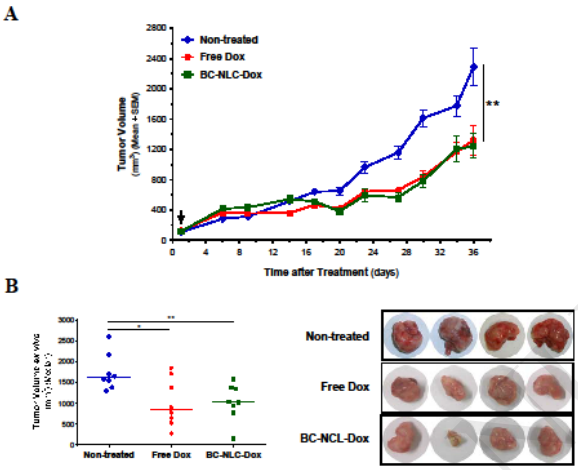

Scheme 1. Different states of Dox. Dox hydrochloride solubilization and ionic equilibrium between Dox mono-cation (Dox-H) and neutral Dox (Dox-N), pKa= 8.46.

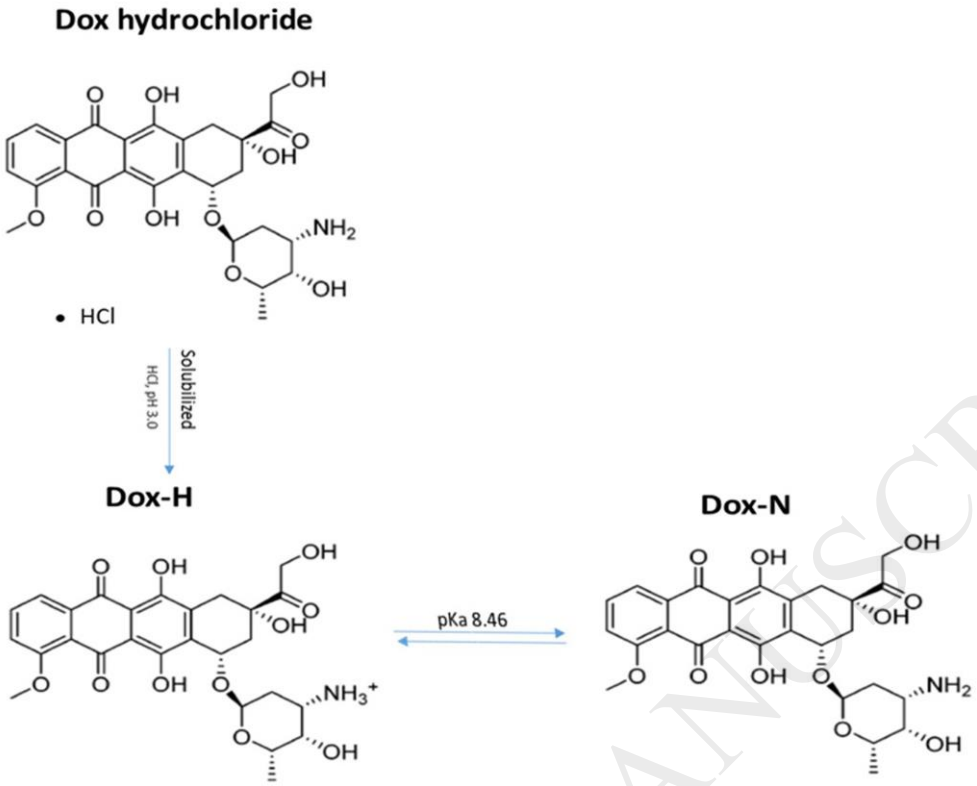

Table 1. NLCs encapsulation efficiency (EE) and characterization by zeta potential (ζ pot), mean diameter and PDI analysis. Results correspond to the mean between three independent experiments, each one made in triplicates.

Formulation	Size (d, nm)	ζ pot (mV)	PDI	EE (%)
NLCs-N	154.3±9.5	+2.33±0.06	0.21±0.043	96.60±0.10
NLCs-H	143.4±1.5	+2.64±0.91	0.170±0.015	48.06±2.68

Table 2. Encapsulation efficiency (EE) for loaded BC films, expressed as encapsulated Dox in µmol per BC film. Results are the mean of two independent experiments, each one performed in quadruplicate, and errors estimated by standard deviation.

System	EE (µmol/film)
BC-Dox	0.043 ± 0.005
BC-NLCs-N	0.147 ± 0.014
BC-NLCs-NH	0.105 ± 0.015

Table 3. Treatment toxicity. Macroscopic observations on tumor site after treatment with free Dox and BC-NLCs-NH films. Inflammation and external necrosis were marked as toxicity incidences.

	Free Dox	BC-NLCs-NH
Inflammation	38%	0%
External necrosis	68%	0%